IOP Publishing Physica Scripta
Phys. Scr. 95 (2020) 045105 (8pp) https://doi.org/10.1088/1402-4896/ab68bb

Tunable optical response of an optomechanical system with two mechanically driven resonators

Amjad Sohail[1], Rizwan Ahmed[2], Chang shui Yu[3], Tariq Munir[1] and Fakhar -e-Alam[1]

[1] Department of Physics, Government Collage University, Allama Iqbal Road, Faisalabad 38000, Pakistan
[2] Physics Division, Pakistan Institute of Nuclear Science and Technology (PINSTECH), P. O. Nilore, Islamabad 45650, Pakistan
[3] School of Physics, Dalian University of Technology, Dalian 116024, People's Republic of China

E-mail: amjadsohail@gcuf.edu.pk

Received 26 June 2019, revised 22 December 2019
Accepted for publication 7 January 2020
Published 18 February 2020

Abstract

We analytically investigate the optical response of an optomechanical system with two mechanical driven resonators which are mutually coupled via Coulomb coupling. We report an efficient scheme to control the optical response by appropriate adjustment of the phase and the intensity of mechanical driving fields. Interestingly, tuning the phase and intensity of the mechanical driving fields lead to the manipulation of the weak probe field which changes its behavior from excessive absorption to significant amplification. In addition, we also show that by applying the driving field to the left (right) mechanical resonator, one can generate the absorption and amplification at the sideband windows (opacity point). Furthermore, the enhanced absorption and amplification strongly depends on whether the phase of mechanical driving fields are in phase or out of phase.

Keywords: OMIT, Coulomb interaction, optomechanical system

(Some figures may appear in colour only in the online journal)

1. Introduction

Cavity optomechanical system (OMS) explores the interaction between light and mechanical modes and has attracted a momentous interest in both the experiment and theory [1–4]. OMS plays a cruicial role in the manipulation of electromagnetic felds and mechanical resonators (MRs), and leads to extensive topics, such as single-photon transport [5], cooling of MRs [6, 7]and optomechanically induced transparency (OMIT) [8, 9]. A typical OMS comprises a Fabry–Perot cavity with one fixed mirror and the other movable or a mechanical membrane oscillating between the two fixed mirror. When a weak probe field and a strong pump field is applied to an OMS, the cavity field is modified due to the radiation pressure force and consequently, the phenomena of OMIT, as an analogue of electromagnetically induced transparency, as an output at the weak detecting field frequency can be observed [10–12].

Recently, the multimode OMSs have attracted a considerable research interest [13–17]. One can achieve the multimode OMS by three ways. Firstly, by combining two optical cavities with equal or unequal resonant frequencies to a single MR, the various phenomena such as multiple OMIT phenomenon [18–20], entanglement [21], normal mode splitting [22] and as optical trimmer [23] can be observed. Secondly, a single optomechanical cavity can be coupled with two or more MRs leading to the double or multi OMIT phenomenon [24–26], the preparation for the two-mode squeezed states [27], the hybridization between mechanical modes [28] and the Fano resonance [29, 30]. Thirdly, an OMS comprising two optical cavities and the two MRs. In such system, either two optical cavities, each contain MRs, are coupled through hoping factor [22] or two OMS are coupled through mechanical coupling [31]. The phenomena of double-OMIT (DOMIT) is very much similar to the two-photon absorption process, which is observed in 4-level

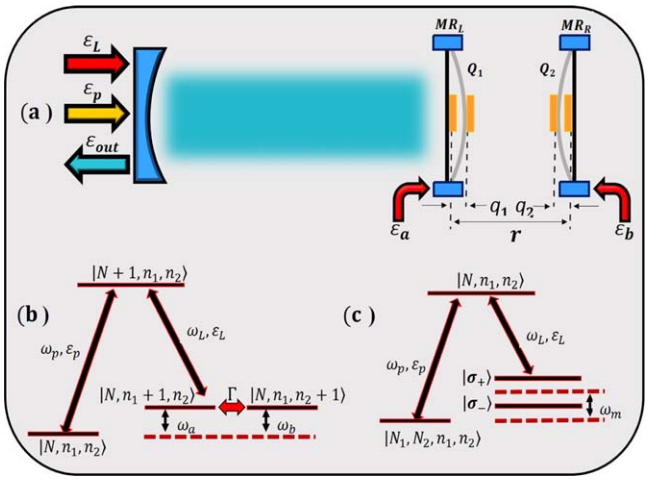

Figure 1. (a) Schematic diagram of the optomechanical system in which the two mechanical resonators MR_L and MR_R are coupled to each other under the action of the Coulomb interaction. The electrode having charge $Q_1(Q_2)$ on $MR_L(MR_R)$ is charged by voltage $V_1(-V_2)$. The equilibrium separation between MR_L and MR_R is r. The small deviation of MR_L and MR_R, due to Coulomb interaction and radiation pressure interaction, from their equilibrium positions are q_1 and q_2 respectively. The cavity is driven by a pump (probe) fields $\varepsilon_L(\varepsilon_p)$. Left mechanical resonator (MR_L) (right mechanical resonator (MR_R)) is driven by external coherently fields with amplitude $\varepsilon_a(\varepsilon_b)$. (b) Schematic of the energy-level diagram in the hybrid cavity OMS, where $|N\rangle$, n_a and n_b denote the number states of the photon inside the cavity, MR_L and MR_R phonons. The transitions $|N, n_a, n_b\rangle \leftrightarrow |N+1, n_a, n_b\rangle$, $|N+1, n_a, n_b\rangle \leftrightarrow |N, n_a+1, n_b\rangle$ and $|N, n_a+1, n_b\rangle \leftrightarrow |N+1, n_a, n_b+1\rangle$ changes the cavity field, caused by the radiation pressure coupling and induced by the Coulomb coupling respectively. (c) Energy level diagram of the hybrid OMS in the dressed-state view. The two dressed states are bring forth by the Coulomb coupling between the two mechanical resonators.

atomic systems [32, 33]. In order to generate the DOMIT, one can couple an additional resonator with the typical OMS as shown by figure 1(a) [25]. This additional resonator form additional level which is now coupled with the original three level structure of a typical OMS to form a four-level energy structure as shown by figures 1(b)–(c). In this way, a DOMIT can be obtained under the quantum interference among different paths.

In present study, we investigate the optical response of the OMS consisting of two driven mechanical resonators which are also mutually coupled via Coulomb force. These mechanical elements are spatially separated by a distance r. In previous reports, an optical response [25] and entanglement [34] of such system was studied by tuning the mechanical frequencies of the two mechanical resonators and observed DOMIT. In addition, they did not use any mechanical driving fields. In contrast, we have studied the optical response by applying mechanical driving fields on the mechanical resonators with equal frequency. Here, instead of only illustrating the DOMIT in our system, we are especially interested in how the optical response of an OMS with two driven mechanical resonator changes its behavior in the presence of Coulomb coupling. We showed that how we can switch from single to DOMIT window in the absence of mechanical driving fields. Once the DOMIT generated, both the phase and the intensity of the two weak coherently mechanical driving fields can be used to further manipulate the propagation of the output field at the probe frequency. Since DOMIT play a key role in double-channel quantum information processing [35], temperature measurement [36], $\wp\tau$ symmetry [37], optical switches [38], high-resolution spectroscopy [25] and so on, we would like to specifically investigate how to generate, control and tune the optomechanically induced absorption (OMIA) and amplification around the sideband windows or around the opacity point when both the resonators are driven by weak coherent field. It is shown that by appropriately adjusting the two mechanical driving fields applied on the mechanical resonators, the probe field can be manipulated from an excessive absorption to a significant amplification.

It is important to mention here that different forms of driving forces could be used. For example, if the mechanical resonators are made-up with piezoelectric materials, one can use piezoelectric forces to drive the mechanical resonators [39–41]. Similarly the mechanical resonators can be driven by Lorentz force when a current-carrying mechanical resonator is positioned in the magnetic field [42, 43]. OMSs with coherently mechanical driving fields have been investigated in many fields, including the implementation of weak force measurement [44], single [45–47] and double [48, 49] OMIA and amplification. In addition, the phonon–phonon coupling can be realized by applying the electrostatic force between the two mechanical resonators [50–52], using a piezoelectric transducer [53] or coupling overhang [54, 55]. Many devices can be put into practice to utilize our scheme in experimentation.

The paper is organized as follows. In section II, we introduce the system and the dynamics by using the quantum Langevin approach. We also solve the system analytically in this section. Next, in section III, we discuss the optical response of the system. In order to study the effect of phase and intensity on the optical response of the system, we present the numerical results in section IV. Finally, we conclude our paper in section V.

2. The model and the dynamics

The system under consideration comprises a Fabry–Perot (FP) cavity and two charged mechanical resonators MR_L and MR_R. The two charged mechanical resonators, at a distance r, are in contact with a thermal bath in equilibrium at temperature T and are coupled through the long range Coulomb interactions as shown schematically in figure 1(a). FP cavity is driven by weak classical probe fields (frequency ω_p) and a strong pump field (frequency ω_L). We describe the optical modes by annihilation (creation) operators $c(c^\dagger)$. The momentum and position operators of the mechanical resonators are represented by p_k and q_k where $k = 1,2$,

respectively. The Hamiltonian of the system is given by

$$H = H_0 + H_{int} + H_{dr}, \tag{1}$$

where

$$\begin{aligned} H_0 &= \hbar\omega_c c^\dagger c + \sum_{k=1,2}\left[\frac{p_k^2}{2m} + \frac{1}{2}m\omega_k^2 q_k^2\right] \\ H_{int} &= -\hbar g c^\dagger c q_1 + H_{\rm CI} \\ H_{dr} &= \mathrm{i}\hbar[\varepsilon_a \hat{b}_1^\dagger \mathrm{e}^{-\mathrm{i}(\omega_a t+\phi_a)} + \varepsilon_b \hat{b}_2^\dagger \mathrm{e}^{-\mathrm{i}(\omega_b t+\phi_b)} + \mathrm{H.c}] \\ &\quad + \mathrm{i}\hbar[(\varepsilon_L \mathrm{e}^{-\mathrm{i}\omega_L t} + \varepsilon_p \mathrm{e}^{-\mathrm{i}(\omega_p t+\phi_p)})c^\dagger + \mathrm{H.c}], \end{aligned} \tag{2}$$

Here, H_0 is the free Hamiltonian comprising the two terms The first term is the self energy of single mode cavity with frequency ω_c and the second term, in the bracket, describes Hamiltonian of the two mechanical resonators. H_{int} represents the interaction Hamiltonian. The first term in H_{int} is the interaction between cavity and the mechanical resonator MR_L with coupling strength g. $H_{\rm CI}$ represents the Coulomb interaction between two charged mechanical resonators MR_L and MR_R. H_{dr} is the Hamiltonian describing the energy of input fields to the system. The first two terms of H_{dr} represent the mechanical driving fields with amplitude ε_a and ε_b which are applied to excite the mechanical resonator MR_L and MR_R respectively. Meanwhile, the cavity is driven by strong pump field with amplitude ε_L and a weak probe field with amplitude ε_p as exhibited by the last two terms in H_{dr}.

We consider the Coulomb coupling between two mechanical resonators MR_L and MR_R and is given as [50, 51]

$$H_{\rm CI} = \frac{-C_1V_1C_2V_2}{4\pi\varepsilon_o|r+q_1-q_2|}, \tag{3}$$

where r is the equilibrium separation between two resonators. The gate size is such that the charge Q_1 (Q_2) on the mechanical resonators MR_L (MR_R) is equal to C_1V_1 ($-C_2V_2$) with $C_1(C_2)$ and $V_1(-V_2)$ being the capacitance and the voltage of the bias gate, respectively. We assume that there is no dependency of V_2 upon Q_1 and vice versa. We also assume that the small oscillations of the charged resonators is much weaker than the distance between the two charged resonators i.e. $q_i \ll r$. The term describing the interaction between two charged resonators can be expanded to the second order as:

$$H_{\rm CI} = \frac{-C_1V_1C_2V_2}{4\pi\varepsilon_o r}\left[1 - \frac{q_1-q_2}{r} + \frac{(q_1-q_2)^2}{r^2}\right]. \tag{4}$$

The linear term can be absorbed into the definition of the equilibrium positions, and the quadratic term includes a renormalization of the oscillation frequency for both resonators MR_L and MR_R. Through further omitting the constant term, the Coulomb interaction term can be written in a simpler from

$$H_{\rm CI} = \hbar\sigma q_1 q_2, \tag{5}$$

where $\sigma = \frac{C_1V_1C_2V_2}{4\pi\varepsilon_o\hbar r^3}$ [25, 56–58]. In the rotating wave approximation at the coupling frequency ω_L, the Hamiltonian of our system can be written as

$$\begin{aligned} H &= \hbar\Delta_0\hat{c}^\dagger\hat{c} + \sum_{k=1,2}\left[\frac{p_k^2}{2m} + \frac{1}{2}m_k\omega_k^2 q_k^2\right] \\ &\quad -\hbar g\hat{c}^\dagger\hat{c}q_1 + \hbar\sigma q_1 q_2 \\ &\quad +\mathrm{i}\hbar[\varepsilon_a\hat{b}_1^\dagger \mathrm{e}^{-\mathrm{i}(\omega_a t+\phi_a)} + \varepsilon_b\hat{b}_2^\dagger \mathrm{e}^{-\mathrm{i}(\omega_b t+\phi_b)} + \mathrm{H.c}] \\ &\quad +\mathrm{i}\hbar[(\varepsilon_L + \varepsilon_p \mathrm{e}^{-\mathrm{i}(\Omega t+\phi_p)})\hat{c}^\dagger + \mathrm{H.c}], \end{aligned} \tag{6}$$

where $\Delta_0 = \omega_c - \omega_L$ and $\Omega = \omega_p - \omega_L$ is the frequency detuning of the probe field from the pump field. With the creation (annihilation) operator $b_k(b_k^\dagger)$, the momentum and position operators of the mechanical resonators can be written as $p_k = \mathrm{i}\sqrt{\frac{\hbar m_k\omega_k}{2}}(\hat{b}_k^\dagger - \hat{b}_k)$, and $q_k = \sqrt{\frac{\hbar}{2m_k\omega_k}}(\hat{b}_k^\dagger + \hat{b}_k)$. The Hamiltonian of the system becomes

$$\begin{aligned} H &= \hbar\Delta_0\hat{c}^\dagger\hat{c} + \sum_{k=1,2}\hbar\omega_k\hat{b}_k^\dagger\hat{b}_k - \hbar g_m\hat{c}^\dagger\hat{c}(\hat{b}_1^\dagger + \hat{b}_1) \\ &\quad +\hbar\Gamma(\hat{b}_1^\dagger + \hat{b}_1)(\hat{b}_2^\dagger + \hat{b}_2) \\ &\quad +\mathrm{i}\hbar[\varepsilon_a\hat{b}_1^\dagger \mathrm{e}^{-\mathrm{i}(\omega_a t+\phi_a)} + \varepsilon_b\hat{b}_2^\dagger \mathrm{e}^{-\mathrm{i}(\omega_b t+\phi_b)} + \mathrm{H.c}] \\ &\quad +\mathrm{i}\hbar[(\varepsilon_L + \varepsilon_p \mathrm{e}^{-\mathrm{i}(\Omega t+\phi_p)})\hat{c}^\dagger + \mathrm{H.c}], \end{aligned} \tag{7}$$

where $g_m = g\sqrt{\frac{\hbar}{2m_1\omega_1}} = \frac{\omega_c}{L}\sqrt{\frac{\hbar}{2m_1\omega_1}}$ is the single-photon opto-mechanical coupling between the optical field mode (photonic mode) and the mechanical mode (phononic mode). Here, ω_c is the intra-cavity frequency and L is the length of the cavity. Furthermore, $\Gamma = \frac{\hbar\sigma}{2\sqrt{m_1m_2\omega_1\omega_2}}$ is the phonon–phonon coupling strength between the resonator MR_L and MR_L. Neglecting the thermal noises and quantum noise terms, the set of nonlinear quantum Langevin equations for this system can be written as

$$\begin{aligned} \dot{\hat{c}} &= -\left(\mathrm{i}\Delta_0 + \frac{\kappa}{2}\right)\hat{c} + \mathrm{i}g_m\hat{c}(\hat{b}_1^\dagger + \hat{b}_1) + \varepsilon_L \\ &\quad + \varepsilon_p \mathrm{e}^{-\mathrm{i}(\Omega t+\phi_p)}, \end{aligned} \tag{8}$$

$$\begin{aligned} \dot{\hat{b}}_1 &= -\left(\mathrm{i}\omega_1 + \frac{\gamma_1}{2}\right)\hat{b}_1 + \mathrm{i}g_m\hat{c}^\dagger\hat{c} - \mathrm{i}\Gamma(\hat{b}_2^\dagger + \hat{b}_2) \\ &\quad + \varepsilon_a \mathrm{e}^{-\mathrm{i}(\omega_a t+\phi_a)}, \end{aligned} \tag{9}$$

$$\begin{aligned} \dot{\hat{b}}_2 &= -\left(\mathrm{i}\omega_2 + \frac{\gamma_2}{2}\right)\hat{b}_2 - \mathrm{i}\Gamma(\hat{b}_1^\dagger + \hat{b}_1) \\ &\quad + \varepsilon_b \mathrm{e}^{-(\mathrm{i}\omega_b t+\phi_b)}, \end{aligned} \tag{10}$$

where κ is the cavity decay rate and $\gamma_1(\gamma_2)$ is the intrinsic damping rates of mechanical resonators b_1 (b_2). Relative to the intensity of controlled field, we assume that the intensities of the weak external mechanical driving fields and the weak probe field satisfies the conditions $|\varepsilon_p| \ll |\varepsilon_c|, |\varepsilon_a| \ll |\varepsilon_c|$ and $|\varepsilon_b| \ll |\varepsilon_c|$. Thus in this case, we can linearize the set of above dynamical equations of the triply driven OMS by assuming each operator is the sum of its mean value and quantum fluctuation i.e., $\hat{O} = O_s + \delta O$, where O denotes any one of these quantities c, b_1 and b_2. The steady state values of the system can be gotten from equations (8)–(10) when $\varepsilon_p \to 0$, $\varepsilon_a \to 0$ and $\varepsilon_b \to 0$

$$c_s = \frac{\varepsilon_L}{\kappa + \mathrm{i}\Delta_c}, \tag{11}$$

$$b_{1s} = \frac{-ig_m|c_s|^2}{\frac{\gamma_1}{2} + i\omega_1 + \frac{8\Gamma^2\omega_1\omega_2}{\left(\frac{\gamma_2}{2}+i\omega_2\right)\left(i\frac{\gamma_1}{2}+\omega_1\right)\left(i\frac{\gamma_2}{2}+\omega_2\right)}},$$
$$\simeq \frac{-ig_m|c_s|^2}{\frac{\gamma_1}{2} + i\omega_1 + \frac{8\Gamma^2}{\left(\frac{\gamma_2}{2}+i\omega_2\right)}}, \quad (12)$$
$$b_{2s} = \frac{-2\Gamma\omega_1}{\left(\omega_2 - i\frac{\gamma_2}{2}\right)\left(\omega_1 - i\frac{\gamma_1}{2}\right)}b_{1s},$$
$$\simeq \frac{-2i\Gamma}{\left(\frac{\gamma_2}{2} + i\omega_2\right)}b_{1s}, \quad (13)$$

where $\Delta_c = \Delta_0 + g_m(b_{1s}^\dagger + b_{1s})$ is the effective cavity detuning including frequency shift due radiation pressure. The corresponding linearized Langevin equations as follow:

$$\delta\dot{c} = -\left(i\Delta_c + \frac{\kappa}{2}\right)\delta c + iG(\delta b_1^\dagger + \delta b_1) + \varepsilon_p e^{-i(\Omega t+\phi_p)}, \quad (14)$$

$$\delta\dot{b}_1 = -\left(i\omega_1 + \frac{\gamma_1}{2}\right)\delta b_1 + i(G\delta c^\dagger + G^*\delta c) - i\Gamma(\delta b_2^\dagger + \delta b_2) + \varepsilon_a e^{-i(\omega_a t+\phi_a)}, \quad (15)$$

$$\delta\dot{b}_2 = -\left(i\omega_2 + \frac{\gamma_2}{2}\right)\delta b_2 - i\Gamma(\delta b_1^\dagger + \delta b_1) + \varepsilon_b e^{-(i\omega_b t+\phi_b)}, \quad (16)$$

where $G = g_m c_s$ represents the effective optomechanical coupling strength which is controlled by the cavity input power $\wp$. We assume that the OMS is operated in the resolved sideband regime, in which $\omega_i \gg \kappa$ $(i = 1,2)$ and also the cavity is driven by the optical pump field at the red sideband $\Delta_c = \omega_1 = \omega_2$. In order to solve the above set of linearized equation, we also assume that $\Omega = \omega_a = \omega_b$, then the fluctuation terms can be solved by introducing the ansatz: $\delta O = O_- e^{-i\Omega t} + O_+ e^{i\Omega t}$ where O_- and O_+ (with $O = c$, b_1, b_2) correspond to the components at the frequencies ω_p and $2\omega_L - \omega_p$ respectively. Upon substituting the above ansatz into equations (14)–(16), we obtain the solution as

$$c_- = \frac{\Lambda\varepsilon_p e^{-i\phi_p} + G\left(\frac{\gamma_2}{2} - i\Delta_2\right)\varepsilon_a e^{-i\phi_a} - G\Gamma\varepsilon_b e^{-i\phi_b}}{\left(\frac{\kappa}{2} - i\Delta\right)\Lambda + |G|^2\left(\frac{\gamma_2}{2} - i\Delta_2\right)}, \quad (17)$$

where

$$\Delta = \Omega - \Delta_c,$$
$$\Delta_{1,2} = \Omega - \omega_{1,2},$$
$$\Lambda = \left(\frac{\gamma_1}{2} - i\Delta_1\right)\left(\frac{\gamma_2}{2} - i\Delta_2\right) + \Gamma^2.$$

3. Optical response of the system

In this section, we will find out the response of the system at the probe frequency which can easily be calculated by the input–output relation [59]

$$\varepsilon_{out} = \kappa_{ex} c_- - \varepsilon_p e^{-i\phi_p}, \quad (18)$$

with external loss rate $\kappa_{ex} = \eta\,\kappa$. κ is the sum of the intrinsic loss rate κ_{in} inside the cavity and external loss rate κ_{ex} at the input mechanical resonator. Here, η is the experimentally adjustable coupling parameter between the external loss rate κ_{ex} and the total decay rate κ. The range of η is $0 \leqslant \eta \leqslant 1$. It is worth mentioning that cavity is overcoupled for $\eta \simeq 1$ and undercoupled for $\eta \ll 1$. The transmission coefficient T_p of the probe field is given by

$$T_p = \frac{\varepsilon_{out}}{\varepsilon_p e^{-i\phi_p}} = \frac{\kappa_{ex} c_- - \varepsilon_p e^{-i\phi_p}}{\varepsilon_p e^{-i\phi_p}} = \frac{\kappa_{ex} c_-}{\varepsilon_p e^{-i\phi_p}} - 1. \quad (19)$$

In order to study the phase dependency on optical response properties for the probe field, we define the total output field at the probing frequency ω_p can be given by

$$\varepsilon_T = \frac{\kappa_{ex} c_-}{\varepsilon_p e^{-i\phi_p}}, = \chi_p + i\tilde{\chi}_p. \quad (20)$$

It is clear that $\chi_p = \mathrm{Re}(\varepsilon_T)$ and $\tilde{\chi}_p = \mathrm{Im}(\varepsilon_T)$ are the in phase and out-of-phase quadratures of the output probe field, representing the absorptive and dispersive behavior of the output probe field, respectively. The output field in a constructive form

$$\varepsilon_T = \kappa_{ex}\left[\frac{\Lambda + G\left(\frac{\gamma_2}{2} - i\Delta_2\right)\beta_a e^{-i\Phi_A} - G\Gamma\beta_b e^{-i\Phi_B}}{\left(\frac{\kappa}{2} - i\Delta\right)\Lambda + |G|^2\left(\frac{\gamma_2}{2} - i\Delta_2\right)}\right], \quad (21)$$

where $\Phi_A = \phi_a - \phi_p$ and $\Phi_B = \phi_b - \phi_p$ are the phase difference between the probe field and the mechanical driving fields. β_a and β_b are the amplitude-ratios between the probe field and external mechanical driving field i.e. $\beta_\mu = \varepsilon_\mu/\varepsilon_p$ $(\mu = a, b)$.

The real part and imaginary part of ε_T describe the absorption and dispersion of the output field at the probe frequency respectively and can be measured via homodyne technique [59]. In the absence of right mechanical driving field i.e. $\varepsilon_b = 0$, equation (21)) can be written as

$$\varepsilon_T = \kappa_{ex}\left[\frac{\Lambda + G\left(\frac{\gamma_2}{2} - i\Delta_2\right)\beta_a e^{-i\Phi_A}}{\left(\frac{\kappa}{2} - i\Delta\right)\Lambda + |G|^2\left(\frac{\gamma_2}{2} - i\Delta_2\right)}\right], \quad (22)$$

Similarly, in the absence of left mechanical driving field i.e. $\varepsilon_a = 0$, equation (21) can be written as

$$\varepsilon_T = \kappa_{ex}\left[\frac{\Lambda - G\Gamma\beta_b e^{-i\Phi_B}}{\left(\frac{\kappa}{2} - i\Delta\right)\Lambda + |G|^2\left(\frac{\gamma_2}{2} - i\Delta_2\right)}\right]. \quad (23)$$

Table 1. Parameters used in recent experiments for the mechanical resonators.

Reference	ω_1	ω_2	γ_1	γ_2	Material
Fan *et al* [13]	6.87 GHz	456.5 MHz	105.5 KHz	8.47 KHz	AlN
Okamoto *et al* [53]	1.845 MHz	1.848 MHz	131.9 Hz	131.9 Hz	GaAs
Lin *et al* [60]	8.3 MHz	13.6 MHz	2.1 MHz	0.11 MHz	SiO_2
Prasad *et al* [61]	243 MHz	420 MHz	2.4 MHz	2.15 MHz	MoS_2
Weaver *et al* [62]	297 KHz	659 KHz	9.42 Hz	6.28 Hz	Si_3N_4
Kuzyk *et al* [63]	436MHz	437 MHz	22 KHz	22.6 KHz	–

4. Effect of phase and intensity on the optical response

In order to give an intuitive illustration of the optical response, we have numerically evaluated the optical response under the effect of Coulomb strength and two mechanical driving fields and viability of enhanced opacity and remarkable amplification. Here we consider the strong coupling regime for which we have assumed $|G| > \sqrt{\kappa\gamma_m/2}$. In this regime, one can easily get the standard OMIT or Autler–Townes splitting spectra if only the probe and the control fields are applied to the system. But when one apply the additional mechanical driving field, the interference between the phonon–photon parametric process and the OMIT process occur and one can obtain the phase-dependent optical response. The first term in equation (21)) represents the standard OMIT response, second term represents the phonon–photon parametric process and the third term represents phonon–phonon parametric process induced by Coulomb coupling Γ and driving the two mechanical resonators. The parameter used in our system are: decay rate of the driven cavity field $\kappa = 0.1\omega_m$, the damping rate of mechanical resonators $\gamma_1 = \gamma_2 = \gamma_m = 0.001\kappa$, $\eta = 0.05$. We plot the power transmission coefficient T_p and the phase quadratures of the output probe fields and evaluate the system by considering the system parameters. We can estimate the feasibility of the choice of numerical values of the Coulomb coupling strength Γ in recent experiment. If we adjust the gate voltage $V_1 = V_2 = 200$V, the capacitance of the gate $C_1 = C_2 = 2.4$nF and the separation between mechanical resonators without Coulomb and optomechanical interaction $r \simeq 2$ mm, in this situation $\Gamma \approx 0.1\kappa$. If we compare the numerical values used in our coupled OMS, it is obvious that our choice of numerical value of Coulomb coupling strength is easily executable in experiments. table. 1 shows more relevant parameters of experimentally achieved coupled MRs.

In figure 2, we plot the absorption Re(ε_T) as a function of Δ/κ and Γ/κ in the absence of external mechanical driving fields. One can easily note that in the absence of Coulomb coupling strength, a single OMIT window appears at $\Delta/\kappa = 0$. The maxima of the single OMIT window depends on the coupling between the cavity and the mechanical resonators. Once the Coulomb coupling appears, the dip of the single OMIT window is split to form DOMIT windows. Since the DOMIT is induced by Coulomb coupling, therefore Coulomb coupling determine the separation between the minima of the DOMIT. Specifically, the distance between the two dips is given by 2Γ. The detailed explanation of single and DOMIT windows have also been studied in [8, 24, 25].

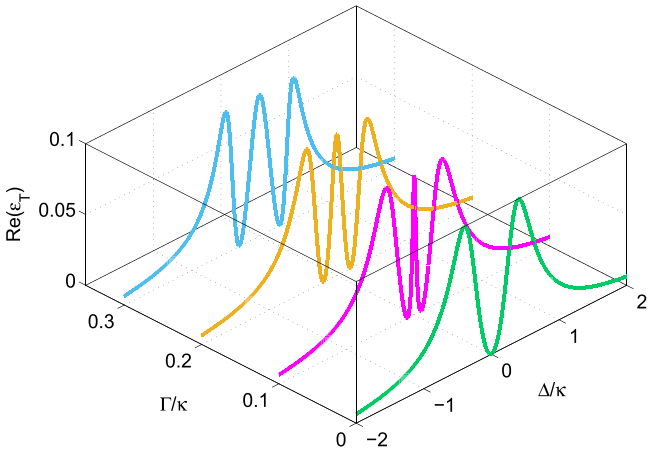

Figure 2. The Real part Re(ε_T) as a function of Δ/κ and Coulomb coupling Γ/κ in the absences of both mechanical driving fields. The other parameters are $\omega_1 = \omega_2 = \omega_m$, $\kappa = 0.1\omega_m$, $\gamma_1 = \gamma_2 = \gamma_m = \kappa/1000$ and $G = 0.5\kappa$.

Left mechanical resonator driven case:- in order to see the effect of phase Φ_A on the optical response in the presence of Coulomb interaction, we plot the power transmission coefficient T_p, absorption Re(ε_T) and dispersion Im(ε_T) versus Δ/κ for different relative phase Φ_A in the presence of Coulomb coupling and in the absence of right mechanical driving field i.e., $\beta_b = 0$ in figures 3(a)–(d). When $\Phi_A = 0$, the interference processes of the two terms in equation (22) slightly suppress the absorption profile around $\Delta/\kappa = 0$ and a symmetric absorption profiles with the maxima at $\Delta/\kappa \simeq \pm 0.5$ is appeared. When $\Phi_A = \pi/2$, we can obtain the gain asymmetric spectra. One can easily observe that in addition to the absorption profile at $\Delta/\kappa = 0$, maxima of the absorption and amplification profiles appear in the red and blue-detunned regions, respectively. When $\Phi_A = \pi$, the Autler–Townes absorption split around $\Delta/\kappa = 0$ and maximum gain appear around $\Delta = \pm 0.1\kappa$. When $\Phi_A = 3\pi/2$, we can get the absorption curve which is almost the mirror image of the absorption curve when $\Phi_A = \pi/2$. The inset in figure 3(a) represent the transmission (absorption) coefficient at $\Delta/\kappa = 0$.

Right mechanical resonator driven case:- now we turn to examine the effect of phase Φ_B on the optical response. We plot the power transmission coefficient T_p, absorption Re(ε_T) and dispersion Im(ε_T) versus Δ/κ for different relative phase Φ_B in figures 4(a)–(d) in the absence of left mechanical driving field

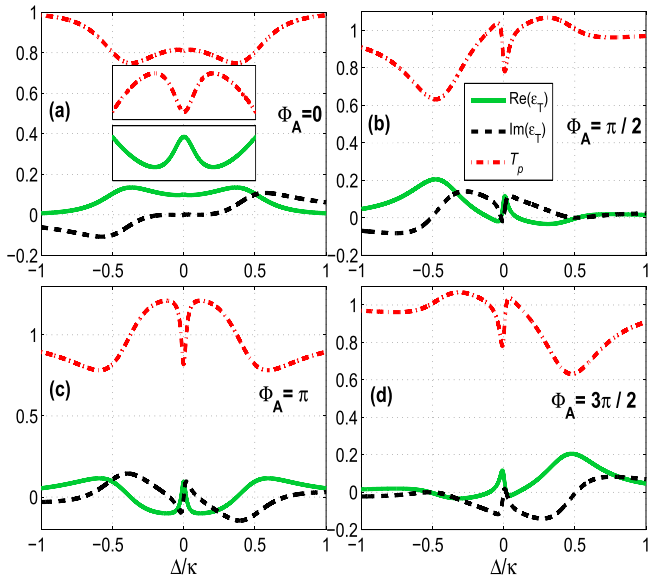

Figure 3. Plots of the phase-dependent power transmission coefficient (dotted–dashed red), absorption (solid green), dispersion (dashed black) versus Δ/κ for different choice of the phase factor (a) $\Phi_A = 0$, (b) $\Phi_A = \pi/2$, (c) $\Phi_A = \pi$ and (d) $\Phi_A = 3\pi/2$. In (a)–(d), $\beta_a = 1$, $\beta_b = 0$. $G = 0.5\kappa$ and $\Gamma = 0.1\kappa$. The inset shows the absorption and transmission curve around Δ/κ. The other parameters are same as in figure 2.

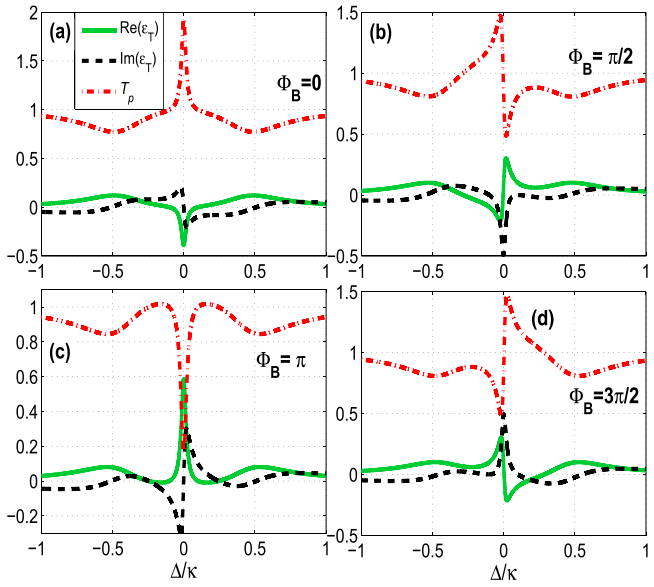

Figure 4. Plots of the phase-dependent power transmission coefficient (dotted–dashed red), absorption (solid green), dispersion (dashed black) versus Δ/κ for different choice of the phase factor (a) $\Phi_B = 0$, (b) $\Phi_B = \pi/2$, (c) $\Phi_B = \pi$ and (d) $\Phi_B = 3\pi/2$. In (a)–(d) $\beta_a = 0$, $\beta_b = 1$, $G = 0.5\kappa$ and $\Gamma = 0.1\kappa$. The other parameters are same as in figure 2.

i.e., $\beta_a = 0$. When $\Phi_B = 0$, the absorption curve is symmetric but the destructive interference between the two terms in equation (23) strongly suppressed the absorption curve at $\Delta/\kappa = 0$. One can easily see that in addition to the maximum absorption at $\Delta = \pm 0.5\kappa$, the absorption curve is strongly amplified at $\Delta/\kappa = 0$ When $\Phi_B = \pi/2$ and $\Phi_B = 3\pi/2$, both the absorption and dispersion profiles are anomalous and exhibit

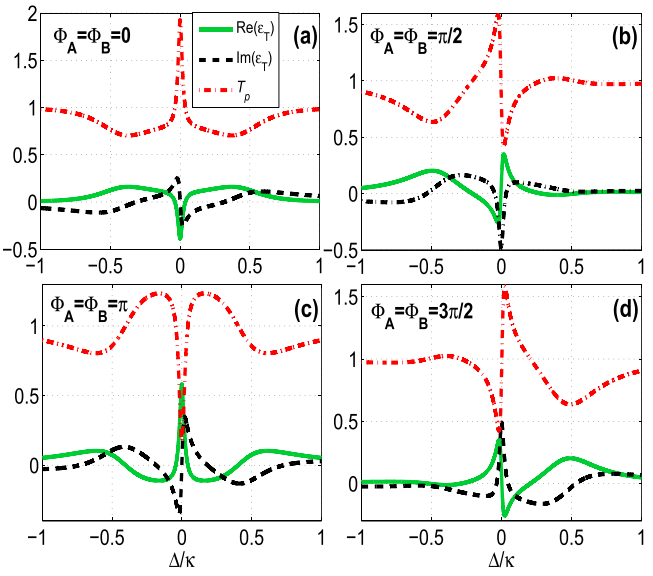

Figure 5. Plots of the phase-dependent power transmission coefficient (dotted–dashed red), absorption (solid green), dispersion (dashed black) versus Δ/κ for different phase factor (a) $\Phi_A = \Phi_B = 0$, (b) $\Phi_A = \Phi_B = \pi/2$, (c) $\Phi_A = \Phi_B = \pi$ and (d) $\Phi_A = \Phi_B = 3\pi/2$. $\beta_a = \beta_b = 1$. The other parameters are same as in figure 2.

the mirror symmetry. Furthermore, one can easily observe the absorption and the dispersion curves in the red-detunned or blue-detunned regions. When $\Phi_B = \pi$, the constructive interference between the two terms in equation (23) strongly enhanced the absorption at the opacity point.

Comparing the above two cases, one can easily observe that when the left mechanical resonator is driven, the absorption from the two side peaks appear when $\Phi_A = 0$ and the amplification from the two dips appeared when $\Phi_A = \pi$. While in the right mechanical driven case, the absorption peak (amplification) occur at the opacity point when $\Phi_B = \pi$ ($\Phi_B = 0$). One can observe the absorption and the amplification is very sharp and narrow around $\Delta/\kappa = 0$. Hence one can easily conclude that the left mechanical driven case can be used to enhance the side peaks of the absorption curve ($\Phi_A = 0$) or amplify the side dips of the absorption curve ($\Phi_A = \pi$). However, the right mechanical driven case can be used to amplify the absorption peak ($\Phi_B = 0$) or enhance the absorption ($\Phi_B = \pi$) around $\Delta/\kappa = 0$.

In figures 5(a)–(d), we plot the power transmission coefficient T_p, absorption Re(ε_T) and dispersion Im(ε_T) versus Δ/κ when both the mechanical driving fields applied on the mechanical resonators are present with equal intensity and phase. One can see that the absorption curve exhibits the combined effect of two mechanical driving fields, which we have separately discussed earlier. Hence, equal contribution of the two mechanical driving fields play an important role to tune the optical response of the OMS.

In order to further explore the effect of two mechanical driving fields more clearly, we plot the absorption spectra as a function of probe detuning for different value of β_a in absence of β_b in figures 6(a)–(b) and for different value of β_b in

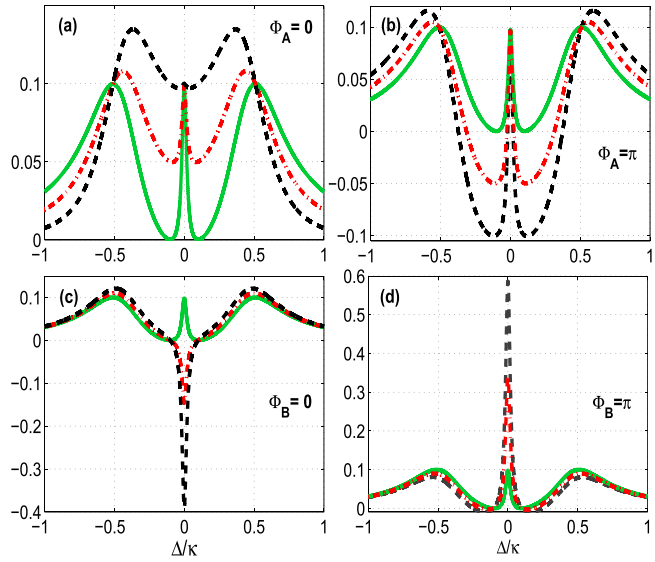

Figure 6. Plots of the absorption Re(ε_T) versus Δ/κ for different phase factor (a) $\Phi_A = 0$ and (b) $\Phi_A = \pi$. In (a),(b), we set $\beta_b = 0$. Here, green solid line represents $\beta_a = 0$, dotted–dashed red line represents $\beta_a = 0.5$, and dashed black line represents $\beta_a = 1$. Plots of the absorption Re(ε_T) versus Δ/κ for different phase factor (c) $\Phi_B = 0$ and (d) $\Phi_B = \pi$. In (c),(d), we set $\beta_a = 0$. Here, solid green line represents $\beta_b = 0$, dotted–dashed red line represents $\beta_b = 0.5$, and dashed black line represents $\beta_b = 1$. The other parameters are same as in figure 2.

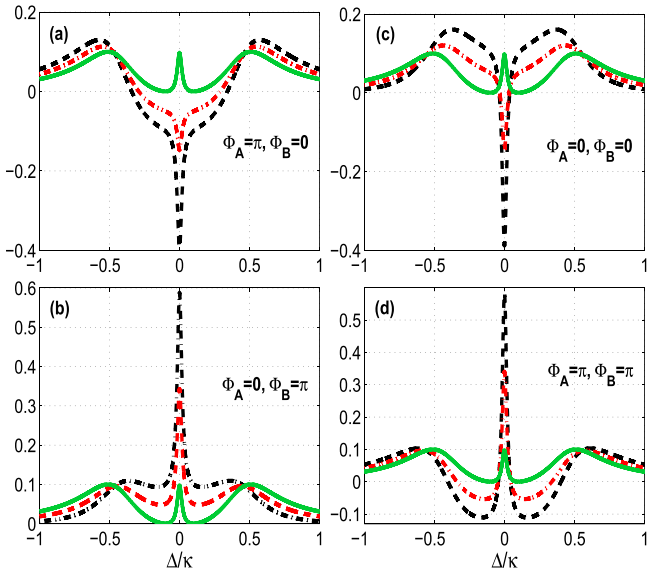

Figure 7. Plots of the absorption Re(ε_T) versus Δ/κ for different phase factor (a) $\Phi_A = \pi$, $\Phi_B = 0$, (b) $\Phi_A = 0$, $\Phi_B = \pi$, (c) $\Phi_A = \Phi_B = 0$ and (d) $\Phi_A = \Phi_B = \pi$. In (a)–(d), figures solid green line represents $\beta_a = \beta_b = 0$, dotted–dashed red line represents $\beta_a = \beta_b = 0.5$, and dashed black line represents $\beta_a = \beta_b = 1$. The other parameters are same as in figure 2.

absence of β_a in figures 6(c)–(d). One can easily see that in the absence of β_a and β_b, a typical DOMIT appears as shown by the solid green line in all subfigures of figure 6. Enhancing the intensity of mechanical driving field β_a when $\Phi_A = 0$, the absorption increase from the two sideband window around $\Delta = \pm\ 0.5\kappa$ as shown in figure 6(a). When $\Phi_A = \pi$, the absorption decrease from the two sideband window around $\Delta = \pm 0.1\kappa$ as shown in figure 6(b). In figures 6(c)–(d), we plot the absorption as function of probe detuning for different value of β_b in absence of β_a. When $\Phi_B = 0$ ($\Phi_B = \pi$), the absorption is decreased (enhanced) monotonically by increasing the amplitude of the mechanical driving field field β_b. Hence, the intensification of left mechanical driving field, the absorption is well modulated from full opacity to enhanced opacity when $\Phi_A = 0$ and from full opacity to significant amplification when $\Phi_A = \pi$ at the two sideband windows. In contrast, the enhancement of right mechanical driving field modulate the absorption curve from full opacity to noteworthy amplification when $\Phi_B = 0$ and from full opacity to excessive opacity when $\Phi_B = \pi$ around $\Delta/\kappa = 0$.

Finally, we discuss the situation when the two mechanical driving fields, with equal intensity, have same or opposite phase. In figure 7(a), we plot the absorption as a function of Δ/κ for $\Phi_A = \pi$ and $\Phi_B = 0$. One can clearly see that not only the absorption curve moved to the amplification side around $\Delta/\kappa = 0$ but also the amplification region become more and more broader as the intensity of the two driving fields increase simultaneously. Next, we consider the situation when $\Phi_A = 0$ and $\Phi_B = \pi$. In this case, not only the complete suppression of the absorption curve around $\Delta = \pm 0.1\kappa$ vanish but also remarkable absorption appear, which monotonically increase with the increase of intensity, around $\Delta/\kappa = 0$ as shown in figure 7(b). Hence, our OMS can be used to generate OMIA. Figures 7(c)–(d) shows the absorption when the phase of the two mechanical driving fields are same. When $\Phi_A = \Phi_B = 0$, the absorption at the two side band due to left mechanical driving and amplification at the opacity point due to right mechanical drive occur at the same time which is well consistent with the figures 6(a) and (c). Similarly when $\Phi_A = \Phi_B = \pi$, absorption at the at the opacity point due to right mechanical driving and amplification at the two side band due to left mechanical driving occur simultaneously which is consistent with the figures 6(b) and (d). Hence, one can conclude that the two mechanical driving fields act oppositely.

5. Conclusion

We, in this study, considered an OMS with two mechanically driven resonators. Our results show that, we can manipulate the response probe field by tuning the phase and the intensities of mechanical resonators. The left mechanical driving field can be used to increase (decrease) the absorption and the amplification of the absorption curve at the sideband windows. However, the right mechanical driving field evolve to display the enhanced absorption and amplification around the opacity point. It is worth noting that when the two mechanical driving fields are out of phase, we can either achieve the OMIA or strong amplification. However, when the mechanical driving fields are in phase, we can get the enhanced absorption or amplification simultaneously. Hence, the phase of the two mechanical driving fields play a vital role and helps to realize our model in

optical switching [64, 65]. Finally, we would like to say that an OMS with two driven mechanical resonators provide great flexibility to control and tune the optical response by controlling the phase and intensity of the mechanical driving fields. Furthermore, our system can also be utilize in high-resolution spectroscopy and multiband optical communications. In addition, it will be beneficial to study the role mechanical driving fields in precision measurements [66, 67], photon blockade [68] and phonon–photon mutual blockade [69].

ORCID iDs

Amjad Sohail https://orcid.org/0000-0001-8777-7928
Chang shui Yu https://orcid.org/0000-0002-8174-3775

References

[1] Aspelmeyer M, Kippenberg T J and Marquardt F 2014 *Rev. Mod. Phys.* **86** 1391–452
[2] Weis S, Rivière, R, Deléglise S, Gavartin E, Arcizet O, Schliesser A and Kippenberg T J 2010 *Science* **330** 1520–3
[3] Fan L, Fong K Y, Poot M and Tang H X 2015 *Nat. Commun.* **6** 5850
[4] Xiong H and Wu Y 2018 *Appl. Phys. Rev.* **5** 031305
[5] Jia W Z and Wang Z D 2013 *Phys. Rev.* A **88** 063821
[6] Gigan S *et al* 2006 *Nature* **444** 67
[7] Schliesser A *et al* 2008 *Nat. Phys.* **4** 415
[8] Agarwal G S and Huang S 2010 *Phys. Rev.* A **81** 041803
[9] Huang S and Agarwal G S 2011 *Phys. Rev.* A **83** 023823
[10] Safavi-Naeini A H, Mayer Alegre T P, Winger M and Painter O 2010 *Appl. Phys. Lett.* **97** 181106
[11] Safavi-Naeini A H, Mayer Alegre T P, Chan J, Eichenfield W, Lin M, Hill Q, Chang D and Painter O 2011 *Nature* **472** 69
[12] Dong C, Fiore V, Kuzyk M C and Wang H 2013 *Phys. Rev.* A **87** 055802
[13] Fan L, Fong K Y, Poot M and Tang H X 2015 *Nat. Commun.* **6** 5850
[14] Seok H, Buchmann L F, Wright E M and Meystre P 2013 *Phys. Rev.* A **88** 063850
[15] Massel F, Cho S U, Pirkkaleinen J M, Hakonen P J, Heikkila T T and Sillanpää M A 2012 *Nat. Commun.* **3** 987
[16] Xu X W, Li Y, Chen A X and Liu Y X 2016 *Phys. Rev.* A **93** 023827
[17] Ma J L, Tan L, Li Q, Gu H Q and Liu W M 2018 *Sci. Rep.* **8** 14367
[18] Hill J T, Safavi-Naeini A H, Chan J and Painter O 2012 *Nat. Commun.* **3** 1196
[19] Sohail A, Zhang Y, Zhang J and Chang-shui Y 2016 *Sci. Rep.* **6** 28830
[20] Andrews R W, Peterson R W, Purdy T P, Cicak K, Simmonds R W, Regal C A and Lehnert K W 2014 *Nat. Phys.* **10** 321
[21] He Y 2015 *Phys. Rev.* A **91** 013827
[22] Hou B P, Wei L F and Wang S J 2015 *Phys. Rev.* A **92** 033829
[23] Li X, Nie W, Chen A and Lan Y 2018 *Phys. Rev.* A **98** 053848
[24] Huang S M 2014 *J. Phys.* B **47** 055504
[25] Ma P C, Zhang J Q, Xiao Y, Feng M and Zhang Z M 2014 *Phys. Rev.* A **90** 043825
[26] Huang S and Tsang M arXiv:1403.1340v1
[27] Woolley M J and Clerk A A 2014 *Phys. Rev.* A **89** 063805
[28] Shkarin A B, Flowers-Jacobs N E, Hoch S W, Kashkanova A D, Deutsch C, Reichel J and Harris J G E 2014 *Phys. Rev. Lett.* **112** 013602
[29] Sohail A, Zhang Y, Bary G and Yu C S 2018 *Int. J. Theor. Phys.* **57** 2814
[30] Ullah K, Jing H and Saif F 2018 *Phys. Rev.* A **97** 033812
[31] Sohail A, Zhang Y, Usman M and Yu C S 2017 *Eur. Phys. J.* D **71** 103
[32] Yan M, Rickey E and Zhu G Y 2001 *Opt. Lett.* **26** 548
[33] Harris S and Yamamoto E Y 1998 *Phys. Rev. Lett.* **81** 3611
[34] Hu X, Hou B P and Tang B 2018 *Optik* **159** 368
[35] Wang H, Gu X, Liu Y X, Miranowicz A and Nori F 2014 *Phys. Rev.* A **90** 023817
[36] Wang Q, Zhang J Q, Ma P C, Yao C M and Feng M 2015 *Phys. Rev.* A **91** 063827
[37] Zhang X Y, Zhou Y H and Guo Y Q 2018 *Phys. Rev.* A **98** 033832
[38] Wu S C, Qin L G, Jing J, Yan T M, Lu J and Wang Z Y 2018 *Phys. Rev.* A **98** 013807
[39] Han X, Zou C L and Tang H X 2016 *Phys. Rev. Lett.* **117** 123603
[40] Cleland A N and Geller M R 2004 *Phys. Rev. Lett.* **93** 070501
[41] Zou C L, Han X, Jiang L and Tang H X 2016 *Phys. Rev.* A **94** 013812
[42] Xue F, Wang Y D, Sun C P, Okamoto H, Yamaguchi H and Semba K 2007 *New J. Phys.* **9** 35
[43] Gaidarzhy A, Zolfagharkhani G, Badzey R L and Mohanty P 2005 *Phys. Rev. Lett.* **94** 030402
[44] Ma J, You C, Si L G, Xiong H, Li J, Yang X and Wu Y 2015 *Sci. Rep.* **5** 11278
[45] Jia W Z, Wei L F, Li Y and Liu Y X 2015 *Phys. Rev.* A **91** 043843
[46] Si L G, Xiong H, Zubairy M S and Wu Y 2017 *Phys. Rev.* A **95** 033803
[47] Xu X W and Li Y 2015 *Phys. Rev.* A **92** 023855
[48] Yang Q, Hou B P and Lai D G 2017 *Opt. Express* **25** 9697
[49] Jinag C, Cui Y S, Zhai Z Y, Yu H L, Li X W and Chen G B 2018 *Opt. Express* **26** 28834
[50] Hensinger W K, Utami D W, Goan H S, Schwab K, Monroe C and Milburn G J 2005 *Phys. Rev.* A **72** 041405 R
[51] Tian L and Zoller P 2004 *Phys. Rev. Lett.* **93** 266403
[52] Luo G, Zhang Z Z, Deng G W, Li H O, Cao G, Xiao M, Guo G C, Tian L and Guo G P 2018 *Nat. Commun.* **9** 383
[53] Okamoto H, Gourgout A, Chang C Y, Onomitsu K, Mahboob I, Chang E Y and Yamaguchi H 2013 *Nat. Phys.* **9** 480
[54] Spletzer M, Raman A, Wu A Q, Xu X and Reifenberger R 2006 *Appl. Phys. Lett.* **88** 254102
[55] Gil-Santos E, Ramos D, Pini V, Calleja M and Tamayo J 2011 *Appl. Phys. Lett.* **98** 123108
[56] Chen R X, Shen L T and Zheng S B 2015 *Phys. Rev.* A **91** 022326
[57] Bai C B, Wang D Y, Wang H F, Zhu A D and Zhang S 2017 *Sci. Rep.* **7** 2545
[58] Nejad A A, Askari H R and Baghshahi H R 2018 *J. Opt. Soc. Am.* B **35** 2237
[59] Walls D F and Milburn G J 1994 *Quantum Optics* (Berlin: Springer) (https://doi.org/10.1007/978-3-540-28574-8)
[60] Lin Q, Rosenberg J, Chang D, Camacho R, Eichen M, Vahala K J and Painter O 2010 *Nat. Photon.* **4** 236
[61] Prasad P, Arora N and Naik A 2019 *Nano Lett.* **19** 5862
[62] Weaver M J, Buters F, Luna F, Eerkens H, Heeck K, Man S D and Bouwmeester D 2017 *Nat. Commun.* **8** 824
[63] Kuzyk M C and Wang H 2017 *Phys. Rev.* A **96** 023860
[64] Deotare P B *et al* 2012 *Nat. Commun.* **3** 846
[65] Andrew M C, Illing L, Susan M C and Daniel J G 2005 *Science* **308** 672
[66] Kong C, Xiong H and Wu Y 2017 *Phys. Rev.* A **95** 033820
[67] Xiong H, Liu Z X and Wu Y 2017 *Opt. Lett.* **42** 3630
[68] Sarma B and Sarma A K 2018 *Sci. Rep.* **8** 14583
[69] Hamsen C, Tolazzi K N, Wilk T and Rempe G 2018 *Nat. Phys.* **14** 885